

Non-collinear magnetic structure and anisotropic magnetoelastic coupling in cobalt pyrovanadate $\text{Co}_2\text{V}_2\text{O}_7$ [†]

W. H. Ji,¹ Y. C. Sun,² C. M. N. Kumar,³ C. Li,⁴ S. Nandi,¹ W. T. Jin,⁵ Y. Su,⁵ X. Sun,¹ Y. Lee,⁶ B. Harmon,⁶ L. Ke,^{6,*} Z. W. Ouyang,^{2,†} Y. Xiao,^{7,‡} and Th. Brückel¹

¹Jülich Centre for Neutron Science JCNS and Peter Grünberg Institut PGI, JARA-FIT, Forschungszentrum Jülich GmbH, 52425 Jülich, Germany

²Wuhan National High Magnetic Field Center, Huazhong University of Science and Technology, Wuhan 430074, P. R. China

³Institut für Festkörperphysik, TU Wien, Wiedner Hauptstr. 8-10/138, 1040 Wien, Austria

⁴Jülich Centre for Neutron Science JCNS, Forschungszentrum Jülich GmbH, Outstation at SNS, POB 2008, 1 Bethel Valley Rd. Oak Ridge, TN 37831-6473, USA

⁵Jülich Centre for Neutron Science JCNS at Heinz Maier-Leibnitz Zentrum, Forschungszentrum Jülich GmbH, Lichtenbergstraße 1, 85747 Garching, Germany

⁶Ames Laboratory, U.S. Department of Energy, Ames, Iowa 50011

⁷School of Advanced Materials, Peking University Shenzhen Graduate School, Shenzhen 518055, China

(Dated: May 16, 2019)

The $\text{Co}_2\text{V}_2\text{O}_7$ is recently reported to exhibit amazing magnetic field-induced magnetization plateaus and ferroelectricity, but its magnetic ground state remains ambiguous due to its structural complexity. Magnetometry measurements, and time-of-flight neutron powder diffraction (NPD) have been employed to study the structural and magnetic properties of $\text{Co}_2\text{V}_2\text{O}_7$, which consists of two non-equivalent Co sites. Upon cooling below the Néel temperature $T_N = 6.3$ K, we observe magnetic Bragg peaks at 2K in NPD which indicated the formation of long range magnetic order of Co^{2+} moments. After symmetry analysis and magnetic structure refinement, we demonstrate that $\text{Co}_2\text{V}_2\text{O}_7$ possesses a complicated non-collinear magnetic ground state with Co moments mainly located in b - c plane and forming a non-collinear spin-chain-like structure along the c -axis. The ab initio calculations demonstrate that the non-collinear magnetic structure is more stable than various ferromagnetic states at low temperature. The non-collinear magnetic structure with canted $\uparrow\uparrow\downarrow\downarrow$ spin configuration is considered as the origin of magnetoelectric coupling in $\text{Co}_2\text{V}_2\text{O}_7$ because the inequivalent exchange striction induced by the spin-exchange interaction between the neighboring spins is the driving force of ferroelectricity. Besides, it is found that the deviation of lattice parameters a and b is opposite below T_N , while the lattice parameter c and β stay almost constant below T_N , evidencing the anisotropic magnetoelastic coupling in $\text{Co}_2\text{V}_2\text{O}_7$.

PACS numbers: 74.70.Xa, 74.62.-c, 75.47.-m, 75.25.Dk

I. INTRODUCTION

Low-dimensional spin systems have attracted extensive interest as their low dimensionality and complex multiple-spin exchange interactions often lead to novel ground states as well as intriguing magnetic behavior, such as spinon excitations in one-dimensional (1D) spin chain system KCuF_3 [1, 2], and a spin liquid state in two-dimensional triangular lattice antiferromagnet NiGa_2S_4 [3]. The complex magnetic and structural characteristics of low-dimensional spin systems will also make its magnetic state highly sensitive to external perturbations including temperature and magnetic field. For instance, the field-induced quantum phase transition from the Néel ordered phase to the spin liquid one is observed in quasi-1D antiferromagnet $\text{BaCo}_2\text{V}_2\text{O}_8$ [4], and a cascade of magnetization plateaus in spin chain system $\text{Ca}_3\text{Co}_2\text{O}_6$ [5–7].

The family of cobalt vanadium oxides $\text{Co}_x\text{V}_2\text{O}_{5+x}$ with $x = (1, 2 \text{ or } 3)$ has attracted special attention due to their complex crystal structure and magnetic behavior, depending on the value of the subscript x [8–11]. The $x = 1$ compound CoV_2O_6 is a low-dimensional spin system which crystallizes in two structural polymorphs with one having a monoclinic unit cell and the other having a triclinic unit cell [12], i.e. α - CoV_2O_6 and γ - CoV_2O_6 . Although two polymorphs pos-

sess different structural symmetries, both α - CoV_2O_6 and γ - CoV_2O_6 are quasi-1D Ising spin-chain compounds. Application of external magnetic field leads to the observation of unusual 1/3 magnetization plateaus in both polymorphs [8, 13–15], which is attributed to the strong spin exchange and the strong coupling between orbital, magnetic and structural orders [16–18]. For $x = 3$, however, the $\text{Co}_3\text{V}_2\text{O}_8$ consists of buckled Kagome layers of edge-sharing CoO_6 octahedra separated by non-magnetic V_5O_4 tetrahedra, showing a geometrically frustrated lattice and a strong two-dimensional magnetic character [19, 20]. Interestingly, a dielectric anomaly is observed around the ferromagnetic (FM) transition temperature T_C indicating the existence of strong coupling between spin and charges in $\text{Co}_3\text{V}_2\text{O}_8$ [21].

When $x = 2$, $\text{Co}_2\text{V}_2\text{O}_7$ adopts a dichromate $\text{K}_2\text{Cr}_2\text{O}_7$ -type structure, which crystallizes in a monoclinic system with space group $P2_1/c$ [22]. As shown in Fig. 1, $\text{Co}_2\text{V}_2\text{O}_7$ possesses two different Co^{2+} sites with two differing local bonding geometries, which are linked in a geometry that can be referred to as a zigzag chain consisting of arrays of edge-shared CoO_6 octahedra. The zigzag chains are interspersed with nonmagnetic V^{5+} in VO_4 pyramid blocks, resulting in a quasi-1D structural arrangement [10]. Touaiher *et al.* [23] reported that $\text{Co}_2\text{V}_2\text{O}_7$ shows a ferromagnetic ordering while

$\text{Ni}_2\text{V}_2\text{O}_7$ shows an antiferromagnetic (AFM) ordering. However, He *et al.* [24] argued that $\text{Co}_2\text{V}_2\text{O}_7$ and $\text{Ni}_2\text{V}_2\text{O}_7$ are likely possessing a similar magnetic ordering since they have the same crystal structure. Recently, two fascinating magnetization plateaus—a 1/2-like plateau and a 3/4 plateau, are observed in $\text{Co}_2\text{V}_2\text{O}_7$, depending on crystallographic directions [25, 26], which is quite different from the isostructural $\text{Ni}_2\text{V}_2\text{O}_7$ with a 1/2 plateau [27]. The first-principles calculations show that the AFM ground state results in a $\uparrow\downarrow\uparrow\downarrow$ -type of spin structure under the assumption that the spin configurations are collinear in the calculations [25]. In addition, magnetic field induced ferroelectricity was reported and found to be correlated with the magnetization plateaus in both $\text{Co}_2\text{V}_2\text{O}_7$ and $\text{Ni}_2\text{V}_2\text{O}_7$ [26]. Moreover, the deviations of the dielectric constant with respect to lattice contributions is evidently observed in $\text{Co}_2\text{V}_2\text{O}_7$ under zero magnetic field, suggesting the appearance of magnetostrictive effects induced by magnetic interactions [28]. Thus, by investigating the magnetic ground state and the response of the lattice to the magnetic phase transitions, it is possible to develop a deeper understanding of the spin-lattice couplings in $\text{Co}_2\text{V}_2\text{O}_7$ [29].

Although there are a few reports on $\text{Co}_2\text{V}_2\text{O}_7$, its magnetic structure remains ambiguous because of the complexity of the structure, which is crucial to understand the field-induced magnetization plateaus, ferroelectricity as well as the magnetostrictive effect. In this paper, we report the structural and magnetic properties of $\text{Co}_2\text{V}_2\text{O}_7$ by magnetization and neutron powder diffraction methods. Both nuclear and magnetic structures are determined through a refinement of high resolution neutron powder diffraction data at low temperature of 2 K. It is found that $\text{Co}_2\text{V}_2\text{O}_7$ exhibits a non-collinear magnetic structure with Co spins forming a canted $\uparrow\uparrow\downarrow\downarrow$ spin chain. The non-collinear magnetic ground state and electronic structure of $\text{Co}_2\text{V}_2\text{O}_7$ can be well understood based on *ab initio* calculations. Moreover, according to the exchange striction model, the appearance of electric polarization can be predicted in $\text{Co}_2\text{V}_2\text{O}_7$ along the chain direction.

II. EXPERIMENTAL METHODS

A. Sample preparation and characterisation

A Polycrystalline sample of $\text{Co}_2\text{V}_2\text{O}_7$ was prepared using the sol-gel method by dissolving stoichiometric amounts of high purity $\text{Co}(\text{NO}_3)_2 \cdot 6\text{H}_2\text{O}$ and NH_4VO_3 in deionized water. The X-ray powder diffraction measurement was carried out on a Huber diffractometer with $\text{Cu K}\alpha$ radiation $\lambda = 1.5406 \text{ \AA}$ and a graphite monochromator. A Quantum Design Physical Property Measurement System (PPMS) was used to characterize the magnetic properties of the $\text{Co}_2\text{V}_2\text{O}_7$ powder sample in the temperature range from 2 to 350 K and the magnetic field range from 0 to 9 T. The temperature dependence of magnetization was measured during warming from 2 to 350 K under 1000 Oe after cooling down from 350 K without the applied field (zero field cooled-ZFC) or under the applied field

(field cooled-FC), while the field dependence of magnetization was measured in magnetic field up to 9 T at selective temperatures.

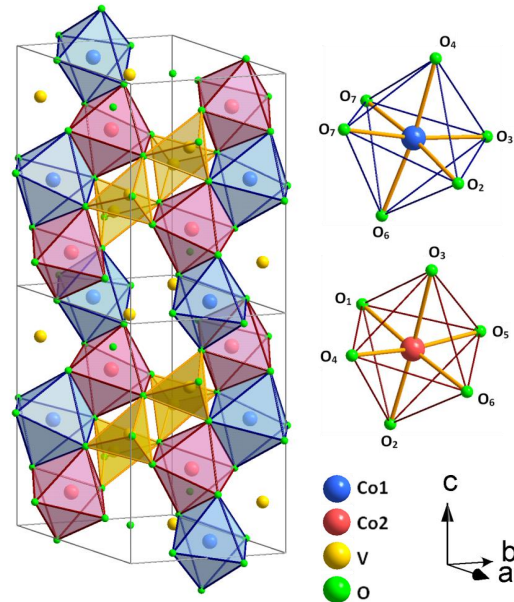


Figure 1: The crystal structure of $\text{Co}_2\text{V}_2\text{O}_7$ at 300 K, which has the prototypical $\text{K}_2\text{Cr}_2\text{O}_7$ -type structure. The crystal structure can be described as the chains of edge-sharing CoO_6 octahedra with VO_4 tetrahedra in between. Two different types of CoO_6 octahedra, i.e. Co_1O_6 and Co_2O_6 , are differentiated by color. The Co-O bond distances of Co_1O_6 and Co_2O_6 are illustrated for comparison.

To study the crystal and magnetic structure of $\text{Co}_2\text{V}_2\text{O}_7$ systematically, time-of-flight (TOF) neutron powder diffraction (NPD) experiments were performed on the high resolution neutron powder diffractometer POWGEN [30] at the Spallation Neutron Source (SNS) in Oak Ridge National Laboratory. About 5 gram of powder sample was loaded in an 8 mm diameter vanadium sample holder and then installed in the helium cryostat that can reach low temperatures down to 2 K. Neutron diffraction data were collected for the $\text{Co}_2\text{V}_2\text{O}_7$ powder sample in the temperature range from 2 to 300 K. For each temperature the data were collected using two different center wavelengths, viz., 1.066 and 3.731 Å to cover a large *d*-space range of 0.5-12 angstrom. The representation analysis were carried out using the program SARAh [31], whereas the crystal and magnetic structure refinements were carried out from the NPD data using the Rietveld refinement program FullProf [32].

B. Calculation details

We have calculated electronic structure, magnetic properties and total energies difference between FM, AFM, and the experimental non-collinear (NC) magnetic states using the Vienna *ab initio* simulation package (VASP) [33, 34]. The nuclei

and core electrons were described by the projector augmented wave (PAW) potential [35]. The wave functions of valence electrons were expanded in a plane-wave basis set with cut-off energy of up to 520 eV. The VASP calculations were performed with 240 k points in IBZ. The correlation effects are also considered by using the generalized gradient approximation (GGA)+ U method [36]. For transition metals, typical U values are between 1.5 to 6 eV [37]. Here, various U parameters between 0 to 4.8 eV are used to investigate the dependence of spin configuration on correlation effects. The experimental lattice parameters and atomic coordinates measured through neutron diffraction at 2K, as listed in Table I, were used in all calculations.

III. EXPERIMENTAL RESULTS AND DISCUSSION

A. Magnetization and magnetic phase transition

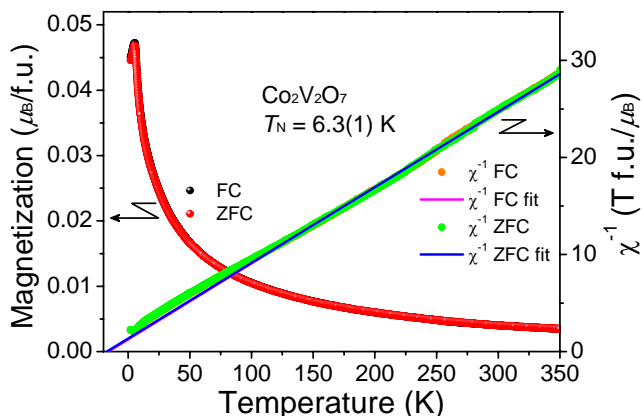


Figure 2: Temperature dependence of the magnetization and inverse magnetic susceptibility χ^{-1} of $\text{Co}_2\text{V}_2\text{O}_7$ measured in zero-field-cooling and field-cooling mode under magnetic field of 1000 Oe. Solid lines indicate Curie-Weiss fits to inverse susceptibility in high temperature region from 200 to 350 K as described in the text.

Figure 2 shows the temperature dependence of the magnetization of the $\text{Co}_2\text{V}_2\text{O}_7$ polycrystalline sample under magnetic fields of 1000 Oe. With decreasing temperature, the magnetization increases smoothly in a temperature range from 350 K to 6.3 K, while it starts decreasing when the sample is cooled below 6.3 K. The phase transition at 6.3(1) K can be clearly observed as indicated by the maximum of the magnetization data. The temperature of 6.3(1) K can be denoted as the Néel temperature T_N where the paramagnetic state develops from the antiferromagnetic phase with increasing temperature, as will be demonstrated by neutron diffraction results in the following text.

Temperature dependence of the inverse susceptibility $1/\chi$ of $\text{Co}_2\text{V}_2\text{O}_7$ compound is also exhibited in Fig. 2. It is known that the magnetic susceptibility of localized noninteracting magnetic ions in high temperature region can be written

as: $\chi(T) = \frac{C}{T - \theta_{CW}}$, where C and θ_{CW} are the Curie constant and Curie-Weiss temperature, respectively. The Curie constant can be expressed as $C = NM_{eff}^2\mu_B^2/3k_B$, where N is the density of magnetic ions, M_{eff} is the effective paramagnetic moment, k_B is the Boltzmann constant, and μ_B is the Bohr magneton. As indicated in Fig. 2, the susceptibility strictly follows the Curie-Weiss behavior in high temperature range, while the inverse susceptibility $1/\chi$ deviated from the Curie-Weiss estimation below 120 K, indicating the onset of considerable magnetic correlations. The effective paramagnetic moment is deduced to be $3.77(1)\mu_B$ and it matches very well with the effective magnetic moment of Co^{2+} , which can be obtained using $p_{eff} = g\sqrt{S(S+1)}$, where $g = 2$ is the Landé g factor and $S = 3/2$. The fit of high temperature susceptibility by means of Curie-Weiss law gives a negative Curie-Weiss temperature of $-16.1(5)$ K, indicating that the dominant magnetic interactions are antiferromagnetic in $\text{Co}_2\text{V}_2\text{O}_7$. Moreover, by comparing the Curie-Weiss temperature θ_{CW} with the Néel temperature T_N , the frustration parameter [38] $f = |\theta_{CW}|/T_N$ is obtained to be 2.5(1), suggesting a moderate spin frustration in $\text{Co}_2\text{V}_2\text{O}_7$.

Figure 3 (a) shows magnetization measured as a function of magnetic field at 2 K. Although the magnetization increase monotonically upon the application of magnetic field, the saturated magnetization still could not be reached upon the application of magnetic field up to 9 T. It is also noticed that a kink takes place at 4.2 T in M - H curve, which suggests that $\text{Co}_2\text{V}_2\text{O}_7$ undergoes a spin-flop transition with increasing magnetic field. The field-induced spin-flop transition is also clearly emphasized in the derivative curve of the magnetization data and it can be considered as the result of competition between Zeeman energy $E = -\mu_0\vec{M}\cdot\vec{H}$ and magnetic anisotropy energy in $\text{Co}_2\text{V}_2\text{O}_7$. The M - H curves at various temperatures are presented in Fig. 3(b). The spin-flop transition can still be observed at 5 K, while it is not discernible once temperature increased to above T_N . Nevertheless, considerable magnetization value, e.g. $2.85\mu_B/f.u.$ at 10 K and 9 T, can still be obtained above T_N , which indicates that the application of a magnetic field can not only change the ordering configuration but also enhances the magnetic ordering temperature of the Co^{2+} moment. With further increase in temperature, the magnetization of $\text{Co}_2\text{V}_2\text{O}_7$ decreased and exhibited typical antiferromagnetic behavior.

B. Crystal structure and non-collinear magnetic ground state determined by NPD

In order to clarify the magnetic ground state of $\text{Co}_2\text{V}_2\text{O}_7$, neutron diffraction patterns were collected in a wide temperature range from 2 to 300 K. Fig. 4 shows the NPD patterns of $\text{Co}_2\text{V}_2\text{O}_7$ at 300 K and 2 K. Two different center wavelengths, i.e. 1.066 and 3.731 Å are applied during the measurements so that a great number of diffraction peaks can be obtained in a large d -space from 0.5 to 12 Å. Two neutron diffraction patterns collected with two different center wave-

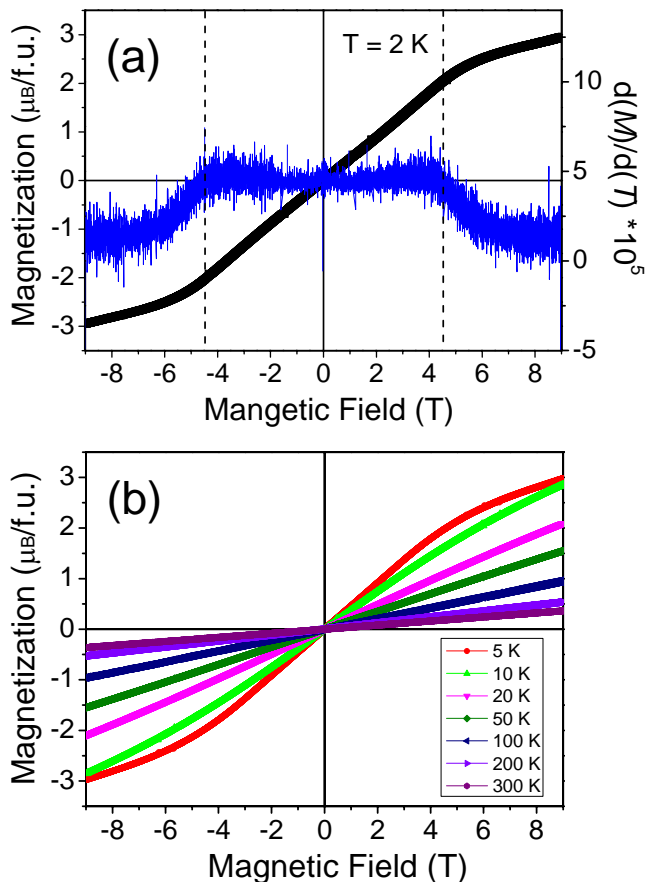


Figure 3: (a) Magnetization as a function of magnetic field for $\text{Co}_2\text{V}_2\text{O}_7$ at 2 K. The dashed line indicates the field-induced spin-flop transition at 4.2 T as determined from the anomaly in the derivative curve of the magnetization. (b) Magnetic field dependence of the magnetization of $\text{Co}_2\text{V}_2\text{O}_7$ measured at different temperatures between 5 and 300 K.

lengths were simultaneously refined for each temperature. At 300 K, $\text{Co}_2\text{V}_2\text{O}_7$ crystallizes in the monoclinic phase with space group $P2_1/c$. By taking advantage of large neutron scattering cross section of Oxygen, the accurate position of Oxygen atom can be easily determined. However, the atomic position of Vanadium can not be determined precisely as the nuclei of Vanadium have a small neutron scattering cross section. Therefore, X-ray diffraction pattern are collected for $\text{Co}_2\text{V}_2\text{O}_7$ at 300 K to determine the atomic position of Vanadium since Vanadium is a strong scatterer of X-rays. The detailed structural information for $\text{Co}_2\text{V}_2\text{O}_7$ at 300 K, as obtained from combining refinement of both NPD and XRD data, are given in Table I. The crystal structure of $\text{Co}_2\text{V}_2\text{O}_7$ and the octahedra of CoO_6 and are illustrated in Fig. 1. The bond length and bond angle of CoO_6 octahedra at 300 K is shown in Table II. The average Co-O bond length of CoO_6 for two nonequivalent Co sites, Co_1 and Co_2 , are 2.074(5) and 2.083(5) Å respectively, indicating a slightly different degree of distortion for these two octahedra. The crystal structure consists two non-equivalent Co sites. With decreasing tem-

perature, the monoclinic structure of $\text{Co}_2\text{V}_2\text{O}_7$ persists down to 2 K accompanied by a shrinkage of lattice. The results of structural refinements at 2 K are also presented in Table I.

In contrast to the NPD patterns at 300 K, extra peaks with considerable intensities show up once the sample was cooled to 2 K, which is below the Néel temperature $T_N = 6.3 \text{ K}$. Most of new emerging peaks possess relatively large d -value and can be assigned as magnetic Bragg peaks, indicating the formation of long range magnetic order of Co^{2+} moments. It is also found that all magnetic reflections can be indexed as commensurate reflections with the magnetic propagation wave vector $\mathbf{k} = (0, 0, 0)$, which means that the magnetic structure is commensurate in nature.

Symmetry analysis allows the determination of the symmetry-allowed magnetic structures based on the representation theory. Magnetic symmetry analysis was carried out for $\text{Co}_2\text{V}_2\text{O}_7$ using the program SARAh [31] by which the allowed symmetry couplings in the form of irreducible representation and their basis vectors can be deduced. It is known that two Co^{2+} ions occupy two inequivalent crystallographic Wyckoff sites $2e$ in $\text{Co}_2\text{V}_2\text{O}_7$ with the crystallographic space group $P2_1/c$. With the commensurate magnetic propagation vector $\mathbf{k} = (0, 0, 0)$, both Co ions are found to have four one-dimensional irreducible magnetic representations (IRs), i.e. $\Gamma_1, \Gamma_2, \Gamma_3, \Gamma_4$, and each of them is composed of three basis vectors (BV) with only real components. Assuming that Co atoms located at two nonequivalent crystallographic sites carry magnetic moments with different amplitude as in $\text{Co}_3\text{V}_2\text{O}_8$ [19] counterpart, all possible IRs are adopted into the magnetic structural model and used to fit against the NPD pattern at 2 K.

As demonstrated in Fig. 4(d), a satisfactory fitting of all magnetic reflections can only be obtained by using IR Γ_2 with Shubnikov space group of $P2_1/c'$, while other three representations can be ruled out due to poor fit of magnetic reflections. The decomposition of the magnetic representation Γ_2 in terms of basis vectors are given in Table III. According to Γ_2 , the Co moments align antiferromagnetically in the magnetic unit cell and the refined vector components of magnetic moment are obtained to be different for two individual Co $2e$ sites, i.e. $m_x = -0.26(5) \mu_B$, $m_y = 1.77(5) \mu_B$ and $m_z = 0.97(5) \mu_B$ for Co_1 site, $m_x = 0.35(5) \mu_B$, $m_y = 2.38(5) \mu_B$ and $m_z = 1.27(5) \mu_B$ for Co_2 site, respectively. It is obvious that the canted Co moments ordered antiferromagnetically in b - c plane and form a spin-chain-like structure along c -axis, as illustrated in Fig. 5. The refined magnetic moments of Co in the spin chain are 2.06(5) and 2.69(5) μ_B for Co_1 and Co_2 , respectively. The canted angle of Co moment toward c -axis is around $26(1)^\circ$. Nevertheless, the tilt of Co spin does not follow the tilt of CoO_6 octahedra, suggesting the negligible influence of electric multipolar field generated by oxygen neighbors on the orbitals of Co ions. The antiferromagnetic ground state of $\text{Co}_2\text{V}_2\text{O}_7$ is apparently determined by the interplay between spin-spin exchange interaction and magnetocrystalline anisotropy, which are largely dependent on the electronic configuration of Co ions. It is known that the

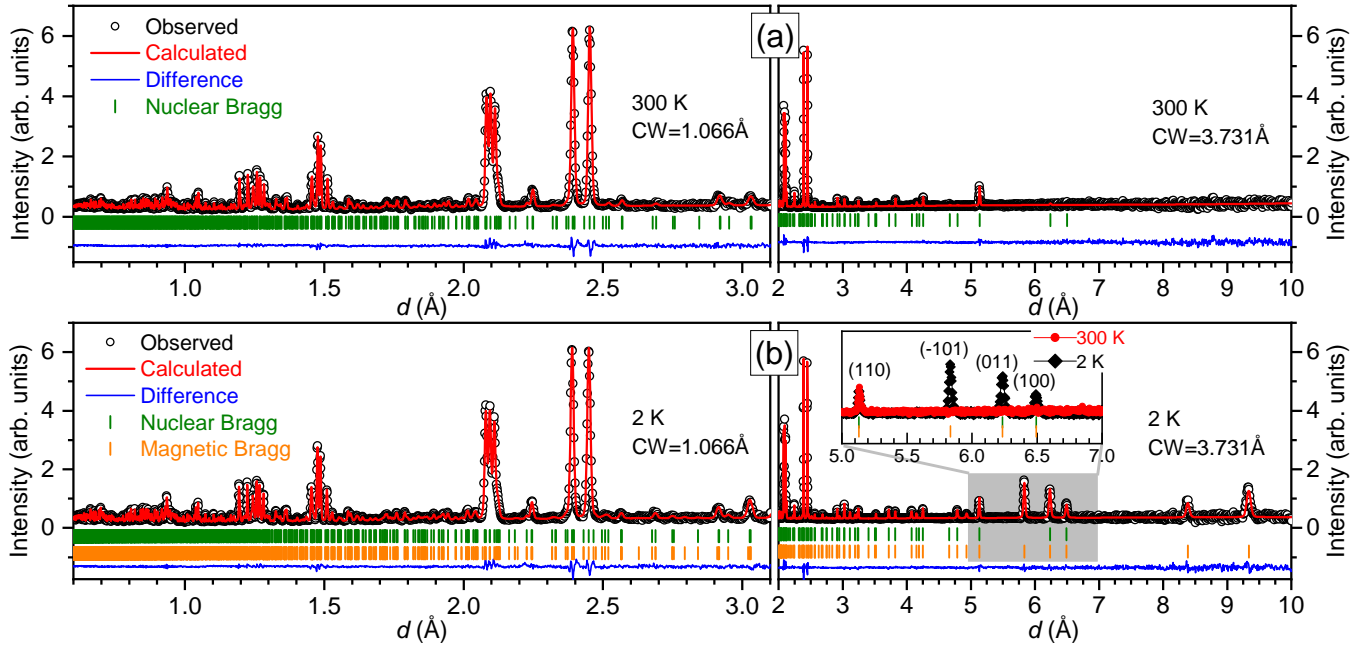


Figure 4: Rietveld refinement results of neutron powder diffraction patterns for $\text{Co}_2\text{V}_2\text{O}_7$ at (a) 300 K and (b) 2 K. The left and right panels show the data collected at the center-wavelength (CW) 1.066 Å and 3.731 Å, respectively. The circles represent the observed intensity and the solid line is the calculated pattern. The difference between the observed and calculated intensities is shown at the bottom. The vertical bars indicate the expected nuclear and magnetic Bragg reflection positions. The inset shows a part of the diffraction pattern for 2 K and 300 K data indicating the additional magnetic reflections upon cooling.

Table I: Crystal structure of $\text{Co}_2\text{V}_2\text{O}_7$, Monoclinic Space group $p2_1/c$

Temperature		300 K					Temperature		2 K				
$a = 6.5932(2)$ Å		$b = 8.3775(2)$ Å		$c = 9.4782(2)$ Å			$a = 6.5860(2)$ Å		$b = 8.3681(2)$ Å		$c = 9.4635(2)$ Å		
$\alpha = 90^\circ$		$\beta = 100.218(2)^\circ$		$\gamma = 90^\circ$			$\alpha = 90^\circ$		$\beta = 100.191(2)^\circ$		$\gamma = 90^\circ$		
Type	Site	x	y	z	B_{iso}		Type	Site	x	y	z	B_{iso}	
Co_1	4e	0.148(3)	0.123(3)	0.463(2)	0.45(2)		Co_1	4e	0.149(3)	0.121(3)	0.469(2)	0.24(1)	
Co_2	4e	0.310(3)	0.382(3)	0.685(2)	0.45(2)		Co_2	4e	0.308(3)	0.389(3)	0.680(2)	0.24(1)	
V_1	4e	0.34(2)	0.75(2)	0.53(2)	0.45(2)		V_1	4e	0.35(2)	0.75(2)	0.53(2)	0.24(1)	
V_2	4e	0.19(2)	0.01(2)	0.81(2)	0.45(2)		V_2	4e	0.18(2)	0.01(2)	0.82(2)	0.24(1)	
O_1	4e	0.604(1)	0.130(1)	0.123(1)	0.55(1)		O_1	4e	0.604(1)	0.130(1)	0.124(1)	0.19(1)	
O_2	4e	0.428(1)	0.126(1)	0.396(1)	0.49(1)		O_2	4e	0.427(1)	0.127(1)	0.395(1)	0.07(1)	
O_3	4e	0.170(1)	0.369(1)	0.461(1)	0.55(2)		O_3	4e	0.176(1)	0.370(1)	0.461(1)	0.16(1)	
O_4	4e	0.255(1)	0.360(1)	0.183(1)	0.37(1)		O_4	4e	0.257(1)	0.359(1)	0.183(1)	0.04(1)	
O_5	4e	0.678(1)	0.373(1)	0.347(1)	0.61(2)		O_5	4e	0.679(1)	0.373(1)	0.348(1)	0.19(1)	
O_6	4e	0.028(1)	0.081(1)	0.246(1)	0.48(1)		O_6	4e	0.028(1)	0.083(1)	0.246(1)	0.12(1)	
O_7	4e	0.852(1)	0.378(1)	0.006(1)	0.52(1)		O_7	4e	0.852(1)	0.379(1)	0.007(1)	0.21(1)	
300 K, 1.066Å		$R_p = 4.03$, $R_{wp} = 5.82$, $\chi = 0.50$					2 K, 1.066Å		$R_p = 4.47$, $R_{wp} = 6.32$, $\chi = 0.58$				
300 K, 3.731Å		$R_p = 3.72$, $R_{wp} = 5.35$, $\chi = 0.15$					2 K, 3.731Å,		$R_p = 5.39$, $R_{wp} = 8.46$, $\chi = 0.39$				

up–up–down–down spin arrangement along the alternating array of two magnetic sites can break the inversion symmetry, and the inequivalent exchange striction working between the up–up (or down–down) spin pair and the up–down (or down–up) can produce electric polarization along the chain direction [39]. Obviously, the exchange-striction mechanism can be applied to $\text{Co}_2\text{V}_2\text{O}_7$ with canted $\uparrow\uparrow\downarrow\downarrow$ spin chains (see Fig. 5) and the electric polarization will emerge as a consequence.

C. Calculation results on magnetic ground state

The calculation started with the experimental spin structure to investigate the electronic structure and magnetic properties of $\text{Co}_2\text{V}_2\text{O}_7$. Two sets of non-collinear calculations are performed: One was with a constraint that fixes Co magnetic moment directions during self-consistent calculations, and the other was without this constraint so that both the directions and magnitudes of each Co magnetic moment were relaxed. Table IV shows the magnetic moment components of each Co

Table II: The bond length and bond angle of CoO₆ octahedra.

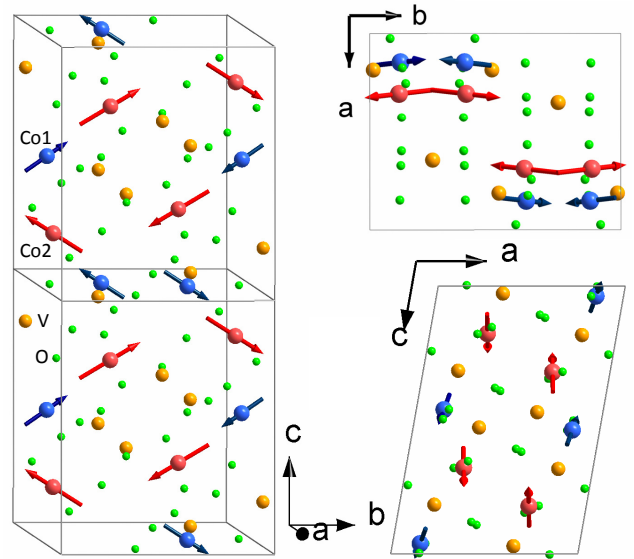
Co ₁	300 K	Co ₂	300 K
O ₂	2.0521 Å	O ₁	2.1298 Å
O ₃	2.0675 Å	O ₂	2.0105 Å
O ₄	2.0878 Å	O ₃	2.1642 Å
O ₆	2.0956 Å	O ₄	2.0663 Å
O ₇	2.0649 Å	O ₅	2.0677 Å
O ₇	2.0746 Å	O ₆	2.0592 Å
O ₂ -Co ₁ -O ₃	85.16 °	O ₁ -Co ₂ -O ₄	96.40 °
O ₂ -Co ₁ -O ₇	94.63 °	O ₁ -Co ₂ -O ₅	87.08 °
O ₃ -Co ₁ -O ₇	94.65 °	O ₄ -Co ₂ -O ₆	88.93 °
O ₇ -Co ₁ -O ₇	86.44 °	O ₅ -Co ₂ -O ₆	87.67 °
O ₄ -Co ₁ -O ₆	173.43 °	O ₂ -Co ₂ -O ₃	174.35 °
Average Co-O bond length			
300 K	Co ₁ -O =2.0737	Co ₂ -O =2.0829	

Table III: Nonzero basis vectors (BV) of the irreducible representations (IR) and positional coordinates for Co atoms that was used to describe the non-collinear magnetic structure of Co₂V₂O₇ with space group $P2_1/c$ and propagation vector $k = (0, 0, 0)$.

IR	BV	Atom	BV Components			Positional coordinates		
			m_{1a}	m_{1b}	m_{1c}	x	y	z
Γ_2	ψ_4	1	1	0	0	x	y	z
		2	-1	0	0	$\bar{x}+1$	$y+\frac{1}{2}$	$\bar{z}+\frac{1}{2}$
		3	-1	0	0	$\bar{x}+1$	$\bar{y}+1$	$\bar{z}+1$
		4	1	0	0	x	$\bar{y}+\frac{1}{2}$	$z+\frac{1}{2}$
	ψ_5	1	0	1	0	x	y	z
		2	0	1	0	$\bar{x}+1$	$y+\frac{1}{2}$	$\bar{z}+\frac{1}{2}$
		3	0	-1	0	$\bar{x}+1$	$\bar{y}+1$	$\bar{z}+1$
		4	0	-1	0	x	$\bar{y}+\frac{1}{2}$	$z+\frac{1}{2}$
	ψ_6	1	0	0	1	x	y	z
		2	0	0	-1	$\bar{x}+1$	$y+\frac{1}{2}$	$\bar{z}+\frac{1}{2}$
		3	0	0	-1	$\bar{x}+1$	$\bar{y}+1$	$\bar{z}+1$
		4	0	0	1	x	$\bar{y}+\frac{1}{2}$	$z+\frac{1}{2}$

atom obtained from NC magnetic calculations with and without relaxing the spin directions. Experimental values are also included to compare. The calculations were carried out using DFT+ U with $U = 3.2$ eV. The calculations show similar magnetic moments for two non-equivalent Co sites while the experiment found noticeably different magnetic moments between two Co sites. The further relaxation of spin direction only introduces small changes on the amplitudes and directions of Co moments, suggesting the obtained spin structure is rather stable.

Atom-projected partial densities of states (PDOS) of the relaxed spin configuration are shown in Fig. 6. The calculations were performed within GGA and GGA+ U with $U = 3.2$ eV, respectively. In the case of $U = 0$ eV, there are sharp Co-DOS peaks near the Fermi energy. The bandgap sits between two sharp DOS peaks, which mostly consist of Co- d states that barely hybridize with other states and form flat bands. The bandgap is about 0.2 eV within GGA and depends on the applied U parameters with GGA+ U . The PDOS with $U = 3.2$ eV are shown in Fig. 6 (b). As expected, a larger bandgap is obtained. It seems that U potential is able to rearrange Co states to promote the hybridization of Co- d states with other states

Figure 5: Illustration of the non-collinear magnetic structure of Co₂V₂O₇ below the magnetic transition temperature. The Co moments ordered antiferromagnetically in b-c plane. The magnetic unit cell is identical to the monoclinic structural unit cell which is outlined with the gray lines.Table IV: Comparison of measured and calculated magnetic moments of two Co sites in Co₂V₂O₇. The Co magnetic moments are in the unit of μ_B .

	Experiment			Constrained			Relaxed		
	m_x	m_y	m_z	m_x	m_y	m_z	m_x	m_y	m_z
Co ₁	-0.260	1.773	0.968	-0.34	2.32	1.27	-0.30	2.33	1.25
	0.260	1.773	-0.968	0.34	2.32	-1.27	0.30	2.33	-1.25
	0.260	-1.773	-0.968	0.34	-2.32	-1.27	0.29	-2.34	-1.25
Co ₂	-0.260	-1.773	0.968	-0.34	-2.32	1.27	-0.30	-2.34	1.24
	0.348	2.376	1.271	0.34	2.33	1.24	0.37	2.37	1.15
	-0.348	-2.376	-1.271	-0.34	-2.33	-1.24	-0.37	-2.38	-1.14
	-0.348	2.376	-1.271	-0.34	2.33	-1.24	-0.36	2.37	-1.15
	0.348	-2.376	1.271	0.34	-2.33	1.24	0.37	-2.37	1.15

so that NC magnetic structure becomes stable. It would be interesting to measure the bandgap, which may guide justifying the U parameter.

Considering that the relaxed spin configuration is not necessary the ground state spin configuration, here, we calculate and compare the total energies of FM, AFM, and NC magnetic structures using VASP. The dependence of these energy differences on the correlation parameter U is also investigated. The plain DFT calculations show that FM state has the lowest energy, which is 3.86 eV/Co and 19.88 eV/Co lower than the AFM state and the NC state, respectively. It is well known that LDA (GGA)+ U method gives better agreement with experimental results than plain LDA (GGA) method for oxide gap materials because of strong correlation. We performed calculations with three different U parameters to understand their effects on the magnetic states. Table V shows the total energies for FM, AFM and NC magnetic structures with vari-

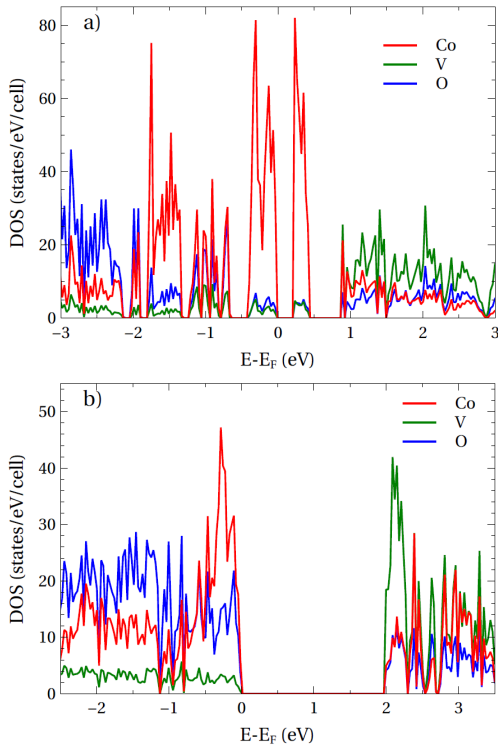


Figure 6: Atom-projected partial densities of states calculated within (a) GGA and (b) GGA+ U with $U = 3.2$ eV.

ous U values. It shows that the magnetic ground state depends on the magnitude of U potential. A larger U parameter tends to stabilize the NC state.

Table V: Calculated total energy (meV/Co) of FM, AFM, and experimental non-collinear (denoted as NC) magnetic states with $U = 0, 1.6, 3.2,$ and 4.8 eV using VASP.

U (eV)	0	1.6	3.2	4.8
FM	0.00	0.00	0.00	0.00
AFM	3.86	-8.59	20.78	18.72
NC	19.88	-7.17	-5.06	-3.18

D. Anisotropic magnetoelastic coupling and thermal expansion

The change of individual lattice parameters with temperature can be obtained through the refinement of NPD patterns collected at different temperatures. As shown in Fig. 7 (a)-(d), the onset of magnetoelastic distortions below $T_N = 6.3$ K is clearly visible for lattice parameters a and b , while the lattice parameter c and β stay almost constant upon crossing the Néel temperature. It is worth noting that the sign of the deviation for a is opposite to that for b , indicating the existence of anisotropic magnetoelastic coupling in $\text{Co}_2\text{V}_2\text{O}_7$. The corresponding unit-cell volume is shown in Fig. 7(e). Although a elongates and b shrinks upon cooling below T_N , they

compensate each other in the volumetric expansion. The unit-cell volume V shows no anomalous change and increases monotonically with temperature.

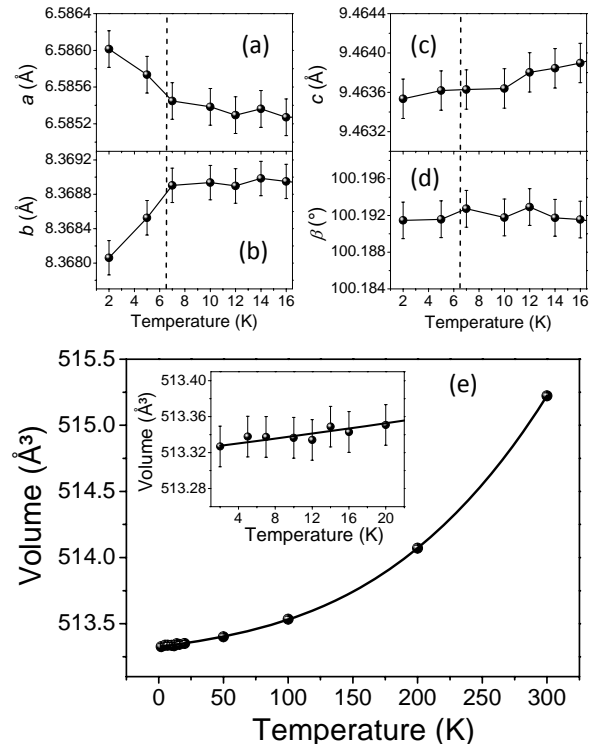


Figure 7: (a)-(d) Temperature dependence of the estimated lattice parameters a, b, c and β . (e) Temperature dependence of the volume of unit-cell of $\text{Co}_2\text{V}_2\text{O}_7$. The inset shows the variation of unit-cell volume in low temperature range.

Because the tilt of Co spin does not follow the tilt of CoO_6 octahedra, we speculate that the influence of electric multipolar field generated by oxygen neighbors on the orbitals of Co ions is negligible. The antiferromagnetic ground state of $\text{Co}_2\text{V}_2\text{O}_7$ is apparently determined by the interplay between spin-spin exchange interaction and single-ion anisotropy. In order to understand anisotropic magnetoelastic coupling and thermal expansion, we correlate the variation of distance between different Co ions in same spin-chain along the c -axis to antiferromagnetic phase transition. The change of distance between neighbouring Co sites at different temperatures is shown in Fig. 8(a). Both of the distance of Co_1 - Co_1 and Co_2 - Co_2 decrease with the increasing of temperature and remain almost constant above T_N . Figure 8(b) display the temperature dependence of the change of distance between different Co sites. According to the non-collinear magnetic structure illustrated in Fig. 5, two non-equivalent Co sites in same spin-chain form parallel or antiparallel spin configurations. The distance of Co_1 - Co_2 with parallel spin ordering shows same behavior as the lattice parameter b , and the distance of Co_1 - Co_2 with antiparallel spin ordering shows same behavior as the lattice parameter a . This is clearly evidence that the anisotropic magnetoelastic coupling and thermal expansion of

lattice parameters are most likely associated with the different exchange interactions between two neighboring Co spins.

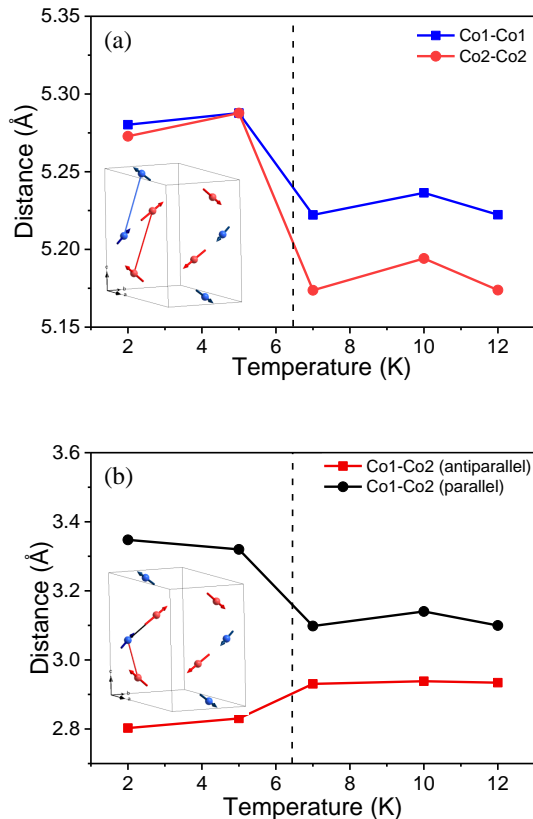


Figure 8: Temperature dependence of the change of distance between different Co ions in same spin-chain along c -axis.

IV. CONCLUSIONS

In summary, we have studied the magnetic properties of $\text{Co}_2\text{V}_2\text{O}_7$ by extensive approaches, such as magnetization measurements, neutron powder diffraction measurements and theoretical calculations. By modeling the temperature dependence of the magnetization with the Curie-Weiss law, we find that the Curie-Weiss temperature is negative, e.g., $-16.1(5)$ K, indicating dominating antiferromagnetic coupling. A spin-flop transition was observed while magnetic field was applied below $T_N = 6.3$ K. By applying neutron powder diffraction methods, we confirm that $\text{Co}_2\text{V}_2\text{O}_7$ remains monoclinic from 300 K down to 2 K. The magnetic ground state was determined unambiguously based on NPD results by using representation analysis combined with magnetic Rietveld refinements. Two non-equivalent Co sites with different magnetic moments form a spin-chain-like structure along c -axis and canted antiferromagnetic ordering in b - c plane. By comparing total energies between different magnetic states, we found

that the theoretical magnetic ground state is sensitive to the U parameter and GGA+ U calculations show that the non-collinear magnetic state possesses a lower energy than FM and AFM states. The ferroelectricity in $\text{Co}_2\text{V}_2\text{O}_7$ can be understood based on exchange striction model, which can be applied to canted $\uparrow\uparrow\downarrow\downarrow$ spin configurations. Moreover, the temperature dependence of lattice parameters in $\text{Co}_2\text{V}_2\text{O}_7$ exhibits an anisotropic magnetoelastic coupling between the a , b and c below T_N .

V. ACKNOWLEDGMENT

This work was supported by the National Natural Science Foundation of China (Grant Nos. 11874023) and Project Based Personnel Exchange Program (PPP) with China Scholarship Council (CSC Nos. 2016-6041) and German Academic Exchange Service (project-id 57219934). Part of the research conducted at SNS was sponsored by the Scientific User Facilities Division, Office of Basic Energy Sciences, US Department of Energy. WHJ would like to acknowledge financial support from the China Scholarship Council(CSC).

* Electronic address: liqinke@ameslab.gov

† Electronic address: zwouyang@mail.hust.edu.cn

‡ Electronic address: xiaoyg@pkusz.edu.cn

- [1] D. A. Tennant, T. G. Perring, R. A. Cowley, and S. E. Nagler, Phys. Rev. Lett. **70**, 4003 (1993).
- [2] B. Lake, D. A. Tennant, C. D. Frost, and S. E. Nagler, Nat. Mater. **4**, 329 (2005).
- [3] S. Nakatsuji, Y. Nambu, H. Tonomura, O. Sakai, S. Jonas, C. Broholm, H. Tsunetsugu, Y. Qiu, and Y. Maeno, Science **309**, 1697 (2005).
- [4] S. Kimura, H. Yashiro, K. Okunishi, M. Hagiwara, Z. He, K. Kindo, T. Taniyama, and M. Itoh, Phys. Rev. Lett. **99**, 087602 (2007).
- [5] P. Lampen, N. S. Bingham, M. H. Phan, H. Srikanth, H. T. Yi, and S. W. Cheong, Phys. Rev. B **89**, 144414 (2014).
- [6] H. Kageyama, K. Yoshimura, K. Kosuge, H. Mitamura, and T. Goto, Journal of the Physical Society of Japan **66**, 1607 (1997).
- [7] Y. B. Kudasov, Phys. Rev. Lett. **96**, 027212 (2006).
- [8] Z. He, J.-I. Yamaura, Y. Ueda, and W. Cheng, Journal of the American Chemical Society **131**, 7554 (2009).
- [9] Y. Drees, S. Agrestini, O. Zaharko, and A. C. Komarek, Crystal Growth and Design **15**, 1168 (2015).
- [10] Z. He, J.-I. Yamaura, Y. Ueda, and W. Cheng, Journal of Solid State Chemistry **182**, 2526 (2009), ISSN 0022-4596.
- [11] G. Balakrishnan, O. A. Petrenko, M. R. Lees, and D. M. c K Paul, Journal of Physics: Condensed Matter **16**, L347 (2004).
- [12] K. Mocala and J. Ziolkowski, Journal of Solid State Chemistry **69**, 299 (1987), ISSN 0022-4596.
- [13] M. Lenertz, J. Alaria, D. Stoeffler, S. Colis, and A. Dinia, The Journal of Physical Chemistry C **115**, 17190 (2011).
- [14] M. Nandi and P. Mandal, Journal of Applied Physics **119**, 133904 (2016).

- [15] H. Shu, Z. Ouyang, Y. Sun, M. Ruan, J. Li, X. Yue, Z. Wang, Z. Xia, and G. Rao, *Journal of Magnetism and Magnetic Materials* **407**, 129 (2016), ISSN 0304-8853.
- [16] F. Wallington, A. M. Arevalo-Lopez, J. W. Taylor, J. R. Stewart, V. Garcia-Sakai, J. P. Attfield, and C. Stock, *Phys. Rev. B* **92**, 125116 (2015).
- [17] N. Hollmann, S. Agrestini, Z. Hu, Z. He, M. Schmidt, C.-Y. Kuo, M. Rotter, A. A. Nugroho, V. Sessi, A. Tanaka, et al., *Phys. Rev. B* **89**, 201101 (2014).
- [18] S. A. J. Kimber, H. Mutka, T. Chatterji, T. Hofmann, P. F. Henry, H. N. Bordallo, D. N. Argyriou, and J. P. Attfield, *Phys. Rev. B* **84**, 104425 (2011).
- [19] Y. Chen, J. W. Lynn, Q. Huang, F. M. Woodward, T. Yildirim, G. Lawes, A. P. Ramirez, N. Rogado, R. J. Cava, A. Aharony, et al., *Phys. Rev. B* **74**, 014430 (2006).
- [20] M. Ramazanoglu, C. P. Adams, J. P. Clancy, A. J. Berlinsky, Z. Yamani, R. Szymczak, H. Szymczak, J. Fink-Finowicki, and B. D. Gaulin, *Phys. Rev. B* **79**, 024417 (2009).
- [21] N. Bellido, C. Martin, C. Simon, and A. Maignan, *Journal of Physics: Condensed Matter* **19**, 056001 (2007).
- [22] E. E. Sauerbrei, R. Faggiani, and C. Calvo, *Acta Crystallographica Section B* **30**, 2907 (1974).
- [23] M. Touaiher, K. Rissouli, K. Benkhouja, M. Taibi, J. Aride, A. Boukhari, and B. Heulin, *Materials chemistry and physics* **85**, 41 (2004).
- [24] Z. He, J.-I. Yamaura, Y. Ueda, and W. Cheng, *Journal of Solid State Chemistry* **182**, 2526 (2009).
- [25] L. Yin, Z. W. Ouyang, J. F. Wang, X. Y. Yue, R. Chen, Z. Z. He, Z. X. Wang, Z. C. Xia, and Y. Liu, *Phys. Rev. B* **99**, 134434 (2019).
- [26] R. Chen, J. F. Wang, Z. W. Ouyang, Z. Z. He, S. M. Wang, L. Lin, J. M. Liu, C. L. Lu, Y. Liu, C. Dong, et al., *Phys. Rev. B* **98**, 184404 (2018).
- [27] Z. W. Ouyang, Y. C. Sun, J. F. Wang, X. Y. Yue, R. Chen, Z. X. Wang, Z. Z. He, Z. C. Xia, Y. Liu, and G. H. Rao, *Phys. Rev. B* **97**, 144406 (2018).
- [28] M. Sanchez-Andujar, S. Yanez-Vilar, J. Mira, N. Biskup, J. Rivas, S. Castro-Garcia, and M. A. Senaris-Rodriguez, *Journal of Applied Physics* **109**, 054106 (2011).
- [29] R. Chen, J. Wang, Z. Ouyang, Z. He, S. Wang, L. Lin, J. Liu, C. Lu, Y. Liu, C. Dong, et al., *Physical Review B* **98**, 184404 (2018).
- [30] A. Huq, J. P. Hodges, O. Gourdon, and L. Heroux, *Zeitsch. Kristall. Proc* **1**, 127 (2011).
- [31] A. Wills, *Physica B: Condensed Matter* **276**, 680 (2000).
- [32] J. Rodríguez-Carvajal, *Physica B: Condensed Matter* **192**, 55 (1993).
- [33] G. Kresse and J. Hafner, *Physical Review B* **47**, 558 (1993).
- [34] G. Kresse et al., *Phys. Rev. B* **54**, 11169 (1996).
- [35] G. Kresse and D. Joubert, *Physical review b* **59**, 1758 (1999).
- [36] S. Dudarev, G. Botton, S. Savrasov, C. Humphreys, and A. Sutton, *Physical Review B* **57**, 1505 (1998).
- [37] E. Şaşıoğlu, C. Friedrich, and S. Blügel, *Physical Review B* **83**, 121101 (2011).
- [38] L. Balents, *Nature* **464**, 199 (2010).
- [39] Y. Tokura, S. Seki, and N. Nagaosa, *Reports on Progress in Physics* **77**, 076501 (2014).

* Electronic address: liqinke@ameslab.gov

† Electronic address: zwouyang@mail.hust.edu.cn

‡ Electronic address: xiaoyg@pkusz.edu.cn